Chapter 8
Modal Analysis of a Second-Gradient Annular Plate made of an Orthogonal Network of Logarithmic Spiral Fibers

Alessandro Ciallella, Francesco D'Annibale, Francesco dell'Isola, Dionisio Del Vescovo, and Ivan Giorgio

Abstract A dynamical study of small vibrations of an annular system made of an orthogonal network of fibers around the undeformed configuration is performed. Logarithmic spirals characterize the net of fibers connected by deformable cylinders. This particular arrangement is chosen because it produces a tough material with an economy of matter.

Key words: Modal analysis · Second gradient surfaces · Homogenized nets · Metamaterials

8.1 Introduction

In this contribution, we analyze the case of a bi-dimensional generalized continuum characterized by a microstructure [1]-[12], which bestows on it high performance, namely high strength with a lightweight. An orthogonal net of curved fibers, i.e., logarithmic spirals, constitutes this microstructure optimized to have one of the most efficient patterns for the structural viewpoint, as established in [13].

Among new manufacturing technologies, 3D printing allows us to build these kinds of microstructured mechanical systems, opening unimaginable possibilities until a

Alessandro Ciallella · Francesco D'Annibale · Francesco dell'Isola · Ivan Giorgio
Department of Civil, Construction-Architectural and Environmental Engineering (DICEAA) & International Research Center on the Mathematics and Mechanics of Complex Systems (M&MoCS), University of L'Aquila, Italy,
e-mail: alessandro.ciallella@univaq.it, francesco.dannibale@univaq.it, francesco.dellisola@univaq.it, ivan.giorgio@univaq.it

Dionisio Del Vescovo
Department of Mechanical and Aerospace Engineering, SAPIENZA Università di Roma, Rome & International Research Center on the Mathematics and Mechanics of Complex Systems (M&MoCS), University of L'Aquila, Italy,
e-mail: dionisio.delvescovo@uniroma1.it

H. Altenbach et al. (eds.), *Sixty Shades of Generalized Continua*,
Advanced Structured Materials 170, https://doi.org/10.1007/978-3-031-26186-2_8

few decades ago [14]-[16]. For this reason, many researchers initiated the set up of systematic methods for synthesizing new micro-structures and, therefore, conceiving novel materials with a macroscopic behavior that fulfills one or more required functionalities. This way of proceeding is typical of a new branch of generalized continua that focuses on designing the so-called metamaterials [17]-[19].

In this contribution, we focus our attention on the dynamic response of the considered system of fibers examining its small vibrations around the undeformed configuration. Locally this fibers network has many features in common with the pantographic sheet [20]. Concerning dynamic behavior, we recall the works by [21]-[26].

This chapter is organized as follows: in Sect. 8.2, we briefly recall the used model to describe the considered network of fibers. In Sect. 8.3, we provide the modal analysis of the system. Finally, in Sect. 8.4, we draw some conclusions and future developments.

8.2 The Model for a Fiber Net Arranged in Logarithmic Spirals

In the continuum mechanics framework, we develop a plate model based on an elastic second gradient theory [27]-[30] to study a mechanical system composed of a network of orthogonal fibers. The aim is to take into account the deformation modes of the fibers that, in a classical plate theory, are not considered, namely, geodesic bending and twisting [3], [31]-[35]. Specifically, the fibers are curved and shaped in the undeformed reference configuration according to logarithmic spirals. To build the net, the fibers are connected with cylindrical pivots, which allow them to have a relative rotation around their pivotal axis [36, 37, 38]. In the examined example, the network is arranged in an annular fashion on a plate (see Fig. 8.1).

According to [35], [39], we define the reference configuration of the elastic surface, $\mathcal{S}$, by the material points $\boldsymbol{X} = (X_1, X_2) \in \Omega \subset \mathbb{R}^2$ that are mapped in the location of the current configuration, $\boldsymbol{x} = (x_1, x_2, x_3) \in \mathbb{R}^3$, by the placement map χ with the standard notation:

$$\boldsymbol{x} = \chi(\boldsymbol{X}) = X_\alpha \boldsymbol{e}_\alpha + u_i(\boldsymbol{X})\boldsymbol{e}_i \tag{8.1}$$

where u_i are the components of the displacement field, the Greek indexes range from 1 to 2, the Latin ones from 1 to 3, being Einstein's convention adopted, and the orthonormal vectors $\{\boldsymbol{e}_i\}$ set as a basis that spans the associated vector space of the Euclidian affine space.

The logarithmic spirals that represent the middle lines of the fibers are parameterized by φ and ψ as follows:

$$\begin{cases} X_1 = R_0\, e^{(\varphi+\psi)} \cos(\varphi - \psi) \\ X_2 = R_0\, e^{(\varphi+\psi)} \sin(\varphi - \psi) \end{cases} \tag{8.2}$$

where R_0 is a constant which specifies the inner radius of the annular plate. In what follows, we adopt the unit-speed parametrization S_β ($\beta = 1,2$) to characterize the two fiber families in the reference configuration given in Eq. (8.2). Therefore, we express the two curvilinear abscissae using the relationships $\varphi = \hat{\varphi}(S_1)$ and $\psi = \hat{\psi}(S_2)$ [39].

The unit tangent vector fields to the fibers in the reference configuration become

$$\boldsymbol{D}_\beta(\boldsymbol{X}) = \frac{\mathrm{d}X_\alpha}{\mathrm{d}S_\beta}\boldsymbol{e}_\alpha \tag{8.3}$$

For the two families of fibers in the reference configuration, we have $\boldsymbol{D}_1 \cdot \boldsymbol{D}_2 = 0$; thus, the fibers are orthogonal. The tangent vectors in the current configuration can be evaluated as

$$\lambda_\beta(\boldsymbol{X})\,\boldsymbol{d}_\beta(\boldsymbol{X}) = \frac{\mathrm{d}\boldsymbol{\chi}}{\mathrm{d}S_\beta}(\boldsymbol{X}) = \boldsymbol{F}(\boldsymbol{X})\,\boldsymbol{D}_\beta(\boldsymbol{X}) \tag{8.4}$$

where $\lambda_\beta = \|\boldsymbol{F}\,\boldsymbol{D}_\beta\|$, $\boldsymbol{F} = \nabla_X \boldsymbol{\chi}$, and $\boldsymbol{d}_\beta$ represent the unit tangent vector fields in the current configuration. The unit vector normal to the surface $\mathcal{S}$ in the current configuration is

$$\boldsymbol{n}(\boldsymbol{X}) = \frac{\boldsymbol{d}_1 \times \boldsymbol{d}_2}{\|\boldsymbol{d}_1 \times \boldsymbol{d}_2\|} \tag{8.5}$$

To fully describe the kinematics of the fibers, we also introduce two rotation tensor fields, one for each fiber family representative of their cross-section orientation as

$$\boldsymbol{R}_\beta : \{\boldsymbol{e}_i\} \mapsto \{\boldsymbol{d}_\beta,\ \boldsymbol{n} \times \boldsymbol{d}_\beta,\ \boldsymbol{n}\} \tag{8.6}$$

and, accordingly, by treating the fibers as an infinite distribution of Kirchhoff's rods [40]-[42], to specify their current geometric features, we define the curvature tensor as follows

$$\boldsymbol{W}_\beta = \boldsymbol{R}_\beta^\top \frac{\mathrm{d}\boldsymbol{R}_\beta}{\mathrm{d}S_\beta} \tag{8.7}$$

The skew-symmetric tensor (8.7), indeed, allow us to define the twisting, out-of-plane, and geodesic curvature, i.e.,

$$\kappa_{T\beta} = \left(\boldsymbol{n} \times \boldsymbol{d}_\beta\right) \cdot \frac{\mathrm{d}\boldsymbol{n}}{\mathrm{d}S_\beta}, \quad \kappa_{n\beta} = \boldsymbol{n} \cdot \frac{\mathrm{d}\boldsymbol{d}_\beta}{\mathrm{d}S_\beta}, \quad \kappa_{g\beta} = -\left(\boldsymbol{n} \times \boldsymbol{d}_\beta\right) \cdot \frac{\mathrm{d}\boldsymbol{d}_\beta}{\mathrm{d}S_\beta} \tag{8.8}$$

respectively. The measures of deformation characterizing the elastic response of the surface $\mathcal{S}$ are: i) the *fiber stretching*, $\varepsilon_\beta = \lambda_\beta - 1$; ii) the *shear distortion angle*, $\gamma = \operatorname{asin}(\boldsymbol{d}_1 \cdot \boldsymbol{d}_2)$; iii) the *curvature change*, $\Delta\kappa_{T\beta} = \kappa_{T\beta}$, $\Delta\kappa_{n\beta} = \kappa_{n\beta}$, $\Delta\kappa_{g\beta} = \kappa_{g\beta} - \kappa^0_{g\beta}$ in which the superscript '0' refers to the reference configuration and, in particular, the reference geodesic curvature is

$$\kappa^0_{g\beta} = -\left(\boldsymbol{e}_3 \times \boldsymbol{D}_\beta\right) \cdot \frac{\mathrm{d}\boldsymbol{D}_\beta}{\mathrm{d}S_\beta} \tag{8.9}$$

The deformation energy can be assumed as a quadratic form in the measures of deformation [39] as a first attempt to model the elastic behavior of the examined fiber net:

$$
\begin{aligned}
2U[\chi(\cdot)] = & \int_\Omega \sum_{\beta=1}^{2} K_{e\beta} \left(\lambda_\beta - 1\right)^2 \mathrm{d}\Omega + \int_\Omega K_s \gamma^2 \mathrm{d}\Omega \\
& + \int_\Omega \sum_{\beta=1}^{2} K_{g\beta} (\kappa_{g\beta} - \kappa_{g\beta}^0)^2 \mathrm{d}\Omega + \int_\Omega \sum_{\beta=1}^{2} K_{n\beta} (\kappa_{n\beta})^2 \mathrm{d}\Omega \\
& + \int_\Omega \sum_{\beta=1}^{2} K_{T\beta} (\kappa_{T\beta})^2 \mathrm{d}\Omega
\end{aligned}
\tag{8.10}
$$

in which $K_{e\beta}$, K_s, $K_{g\beta}$, $K_{n\beta}$, and $K_{T\beta}$ are material stiffnesses related to stretching, shearing, geodesic and normal bending, and twisting, respectively. They are evaluated by the expressions:

$$
\begin{aligned}
K_e &= \eta_e \frac{YA}{p}, \quad K_s = \eta_s \frac{GJ_p}{h_p\, p^2}, \quad K_T = \eta_T \frac{GJ_t}{p}, \\
K_g &= \eta_g \frac{YJ_{fg}}{p}, \quad K_n = \eta_n \frac{YJ_{fn}}{p}
\end{aligned}
\tag{8.11}
$$

borrowed by the beam theory. Since the hypotheses behind these expressions are not adequately satisfied, we introduce corrective coefficients, η_i, to overtake this issue. Moreover, A is the area of the fibers cross-section, $J_t = 0.196\, h^3\, b$ and $J_{fn} = h^3\, b/12, J_{fg} = b^3\, h/12$ are the torsional, the out-of-plane and in-plane bending second moment of area of the fiber cross-sections, respectively; $J_p = \pi\, r_p^4/2$ is the torsional second moment of area of the pivot. Because the two families of fibers are equal, so the related stiffnesses are. The variable pitch between two adjacent fibers is denoted by p.

To define the kinetic energy of the plate, we introduce the skew tensor

$$
\boldsymbol{V}_\beta = \boldsymbol{R}_\beta^\top \dot{\boldsymbol{R}}_\beta \tag{8.12}
$$

where the dot denotes differentiation with respect to the time. The significant components of the tensor (8.12) are the angular velocity fields of the cross-section of the fibers, in detail

$$
\omega_{\beta 1} = \left(\boldsymbol{n} \times \boldsymbol{d}_\beta\right) \cdot \dot{\boldsymbol{n}}; \quad \omega_{\beta 2} = \boldsymbol{n} \cdot \dot{\boldsymbol{d}}_\beta; \quad \omega_{\beta 3} = -\left(\boldsymbol{n} \times \boldsymbol{d}_\beta\right) \cdot \dot{\boldsymbol{d}}_\beta \tag{8.13}
$$

Therefore, the kinetic energy of the equivalent continuum annular plate can be evaluated by

$$
\begin{aligned}
2T[\chi(\cdot), \dot{\chi}(\cdot)] = & \int_\Omega \varrho_s (\dot{u}_1^2 + \dot{u}_2^2 + \dot{u}_3^2) \mathrm{d}\Omega \\
& + \int_\Omega \sum_{\beta=1}^{2} \left[J_{\beta 1} (\omega_{\beta 1})^2 + J_{\beta 2} (\omega_{\beta 2})^2 + J_{\beta 3} (\omega_{\beta 3})^2 \right] \mathrm{d}\Omega
\end{aligned}
\tag{8.14}
$$

where ϱ_s is the apparent mass density per unit area, J_i (the same for the two families of fibers) are related to the inertia of the cross-section of fibers and can be evaluated by the expression $\varrho I_i/p$, being ϱ the apparent mass density per unit volume, I_i the second moments of area with respect to the directions $\boldsymbol{D}_1$, $\boldsymbol{D}_2$, $\boldsymbol{e}_3$.

The governing equation of the annular plate, therefore, can be deduced by the stationary-action principle, using the Lagrangian function $\mathscr{L} = U - T$.

8.3 Modal Analysis

In this section, we evaluate the vibration modes of an annular plate made of a logarithmic spiral network of fibers using the second-gradient bi-dimensional model, linearized around the undeformed configuration.

The modal shapes are evaluated using the finite element software COMSOL Multiphysics, which allows the straightforward implementation of the Lagrangian function, $\mathscr{L}$, based on Eq. (8.10) and (8.14). The finite element discretization employs the Argyris elements since the model is two-dimensional and is characterized by a second-gradient elastic theory. In this context, it is paramount to use interpolating functions in the Sobolev space H^2. The same problem might be solved more efficiently with an *ad hoc* homemade code via the isogeometric formulation [43]-[48], discrete Hencky models based on the geometry of the microstructure of the fibers, as done in [49]-[54], or alternatively, as recently proposed, based on swarm robotics [55], [56].

Specifically, a representative sample of an annular plate is investigated. The fibers are assumed to have a rectangular cross-section of size $b \times h$, being $b = 1.6$ mm the base and $h = 1$ mm the height. They are linked together by cylindrical pivots having radius $r_p = 0.45$ mm and height $h_p = 1$ mm. The radius of the inner circle is set to be $R_0 = 50$ mm and the outer radius is $R_e = 260$ mm. The pitch p is geometrically evaluated from a 3D CAD model as shown in Fig. 8.1 by considering the positions of the barycenters of the pivots. In particular, this parameter is characterized by a linear dependence on the annular plate radius according to the relationship:

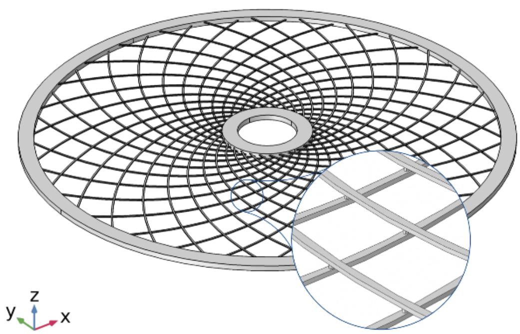

Fig. 8.1 A net prototype feasible with 3D printing.

$$p = m\sqrt{2\left({X_1}^2 + {X_2}^2\right)} + q \tag{8.15}$$

in which $q = -4 \times 10^{-2}$ mm and $m = 0.1085$.

The coefficients η_i conceived to correct the material stiffnesses are estimated by a fitting procedure made with the aim of reproducing the same modal shapes and natural frequencies of a more refined three-dimensional elastic model (see, e.g., [57], [58] for a similar approach). The obtained values are listed in Table 8.1. We assumed the material of the annular plate to be polyamide, homogeneous, and isotropic. It is characterized by Young's modulus $Y = 1600$ MPa and Poisson's ratio $\nu = 0.4$.

The apparent mass density per unit area ϱ_s, clearly not uniform, is also estimated using the 3D CAD model. The idea is to divide the annular plate into a large number of parts within cylindrical annuli, evaluate the mass of each piece, and divide it by the equivalent area of the underlying surface. The result of such a procedure is reported in Fig. 8.2 as a function of the radius because of the symmetry of the geometry.

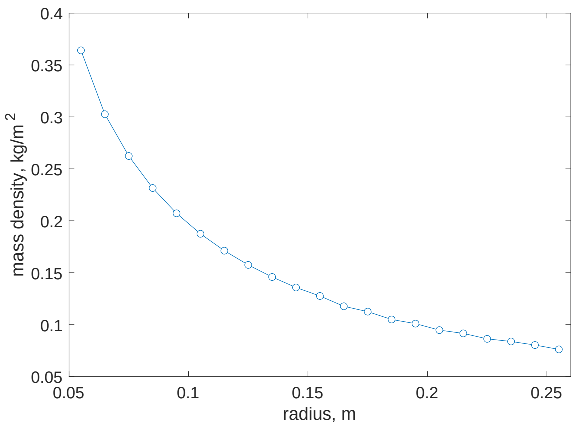

Fig. 8.2 Apparent mass density per unit area vs. radius of the annular plate.

The first twelve modal shapes associated with their natural frequencies are determined and shown in Figs. 8.3–8.5. The out-of-plane displacement is displayed by color in the figures. In the same pictures, we also exhibit the same results obtained with a refined three-dimensional model to assess the correctness of the proposed model in capturing the dynamical behavior of the considered system. Table 8.2 reports the eigenfrequencies for both cases analyzed and compares them with the corresponding errors.

Table 8.1: The fitted coefficients η.

η_e	η_s	η_g	η_n	η_T
1.0	1.0	0.8	1.9	0.8

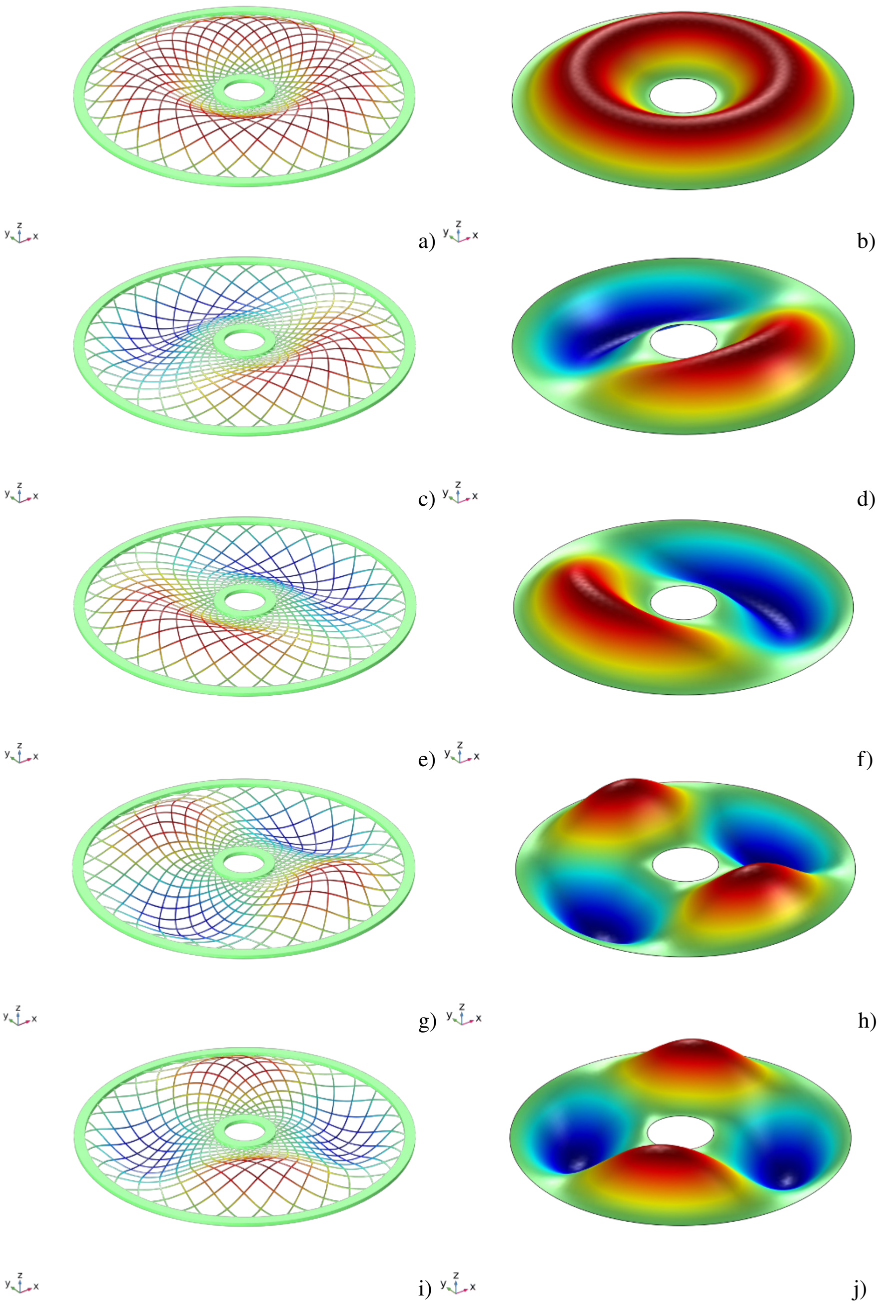

Fig. 8.3: Modal shapes from the first to the fifth, comparison between a 3D model (a, c, e, g, i) and the reduced 2D model (b, d, f, h, j).

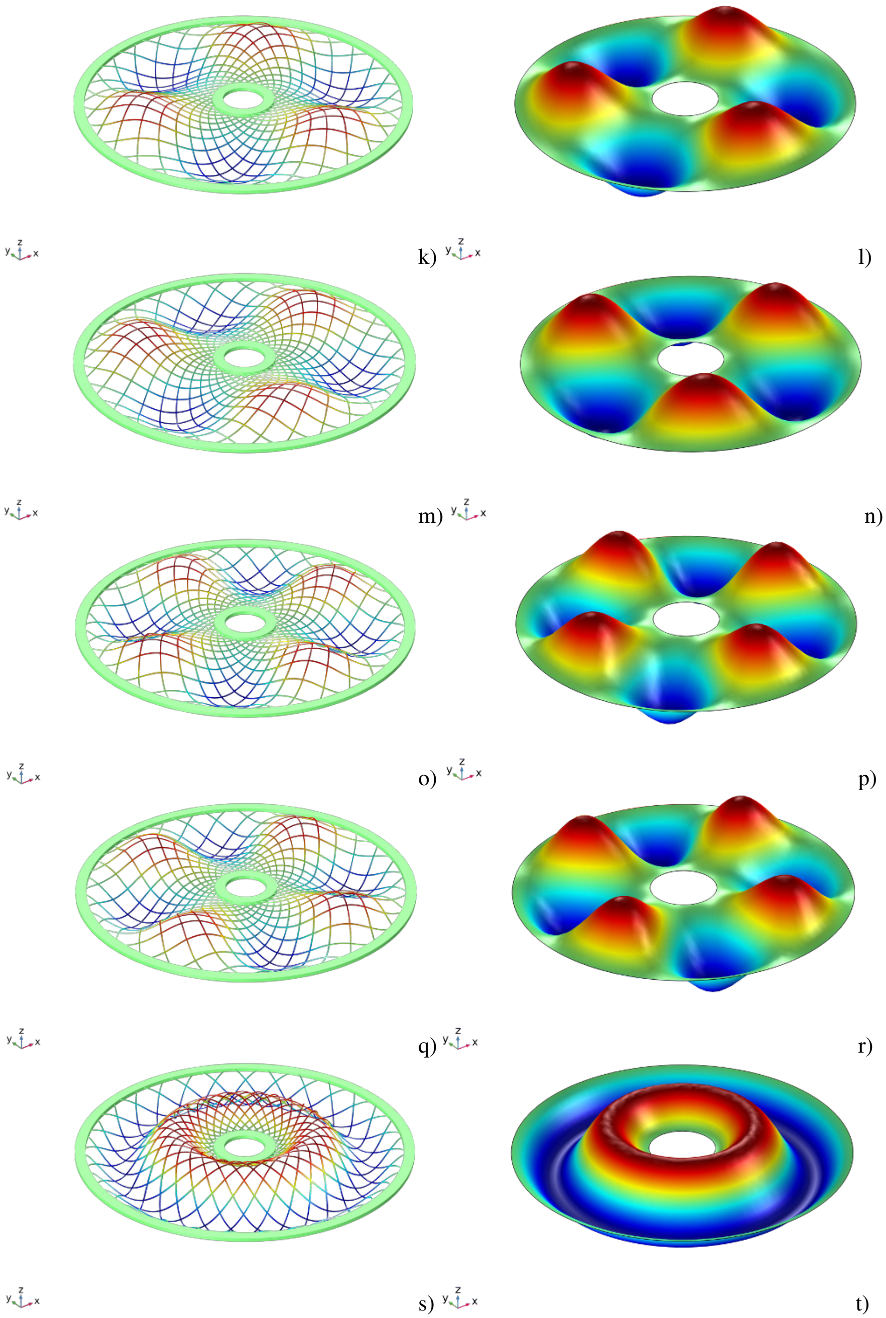

Fig. 8.4: Modal shapes from the sixth to the tenth, comparison between a 3D model (k, m, o, q, s) and the reduced 2D model (l, n, p, r, t).

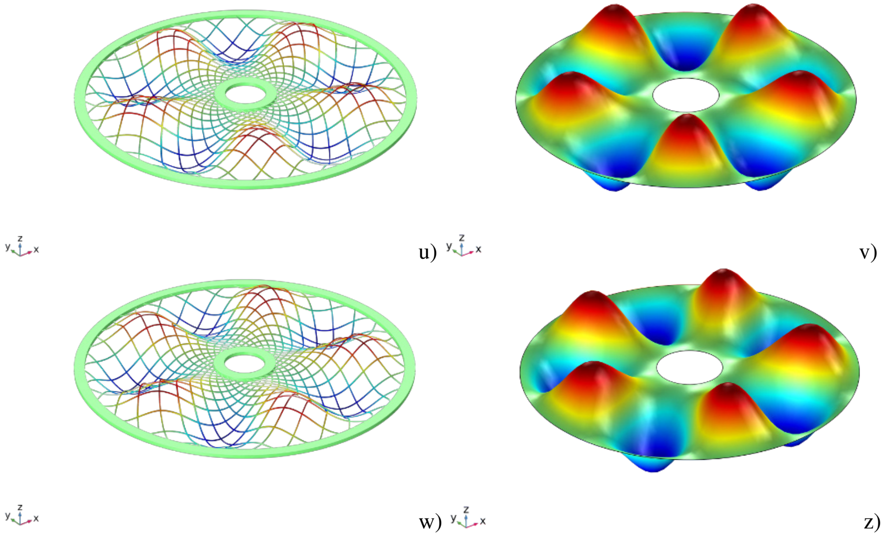

Fig. 8.5: Modal shapes from the eleventh to the twelfth, comparison between a 3D model (u, w) and the reduced 2D model (v, z).

These results show an excellent agreement for the modal shapes. The natural frequencies are rather close for the two models considered for the first seven modes; the others are still close, but a more considerable discrepancy is detected for the remaining modes. These more significant errors, however, can be easily explained by comparing the length of the unit cell of the network to be homogenized with the wavelength of the modal shape. By increasing the frequency, these two quantities become of a compatible magnitude; therefore, the continuum approach is less suitable for accurately describing the annular plate behavior. Besides, the fact that the qualitative behavior is well captured, after all confirms some results obtained for wide-knit pantographic structures [59], even though in a static regime.

Table 8.2: Natural eigenfrequencies, rad/s.

Mode #	3D model	2D reduced model	difference %
1	167.86	162.37	-3.27
2, 3	180.86	174.13	-3.72
4, 5	221.52	210.42	-5.01
6, 7	272.79	271.41	-0.51
8, 9	322.73	353.95	9.67
10	382.55	436.73	14.16
11, 12	385.38	453.67	17.70

8.4 Conclusions and Future Perspectives

In this work, the possibility of using a bi-dimensional second gradient model to describe the small oscillations of a network of curved fibers around its undeformed configuration has been examined. The fibers are characterized by a pattern that, in the reference configuration, is given by logarithmic spirals connected by a weak joint. The results are encouraging since the dynamical response of such a model closely reproduces the behavior obtained by a more refined 3D elastic model, at least for the first modes where the homogenized formulation is significant.

However, if we compare the fitting based on the dynamic quantities, i.e., modal shapes and natural frequencies, with the one obtained by static tests, we notice that the coefficients involving the flexural and twisting behavior of the fibers show some differences [39]. This difference in the results of the regression for the stiffnesses is an index of some issues in the proposed model. Indeed, a consistent model must produce the same material parameters in a dynamic or a static regime. Analyzing the nature of the difference, namely related to the flexural and twisting deformation of the fibers and the current shape of the fibers in the considered modal shapes (see Fig. 8.6), it seems reasonable that the coupling between the twisting of a fiber and the bending of the connected fiber plays a considerable role in the behavior of such a system. This observation leads us to believe that the diagonal constitutive behavior given by Eq. (8.10) is too simplistic in this case. Therefore, we plan to examine, both in static and dynamic regimes, coupling constitutive behaviors between the flexural and twisting energy contributions of fibers as future developments to see if employing more comprehensive energy could overcome the detected discrepancy.

Acknowledgements The authors express their gratitude to Victor Eremeyev for the stimulating discussions and his friendly criticism.

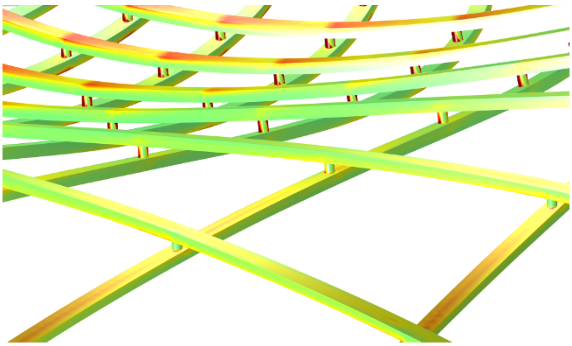

Fig. 8.6 Zoom of a modal shape where a flexion-torsion coupling appears.

References

[1] Eremeyev VA, Pietraszkiewicz W (2016) Material symmetry group and constitutive equations of micropolar anisotropic elastic solids, Mathematics and Mechanics of Solids **21**(2):210-221.

[2] Eremeyev VA (2018) On the material symmetry group for micromorphic media with applications to granular materials, Mechanics Research Communications **94**:8-12.

[3] Eremeyev VA, dell'Isola F, Boutin C, Steigmann D (2018) Linear pantographic sheets: existence and uniqueness of weak solutions, Journal of Elasticity **132**(2):175-196.

[4] Altenbach H, Eremeyev VA, Naumenko K (2015) On the use of the first order shear deformation plate theory for the analysis of three-layer plates with thin soft core layer, ZAMM-Zeitschrift für Angewandte Mathematik und Mechanik **95**(10):1004-1011.

[5] Altenbach H, Eremeyev VA (2011) On the shell theory on the nanoscale with surface stresses, International Journal of Engineering Science **49**(12):1294-1301.

[6] Altenbach J, Altenbach H, Eremeyev VA (2010) On generalized Cosserat-type theories of plates and shells: a short review and bibliography, Archive of Applied Mechanics **80**(1):73-92.

[7] Altenbach H, Eremeyev VA (2008) Analysis of the viscoelastic behavior of plates made of functionally graded materials, ZAMM-Zeitschrift für Angewandte Mathematik und Mechanik **88**(5):332-341.

[8] Altenbach H, Eremeyev VA (2008) Direct approach-based analysis of plates composed of functionally graded materials, Archive of Applied Mechanics **78**(10):775-794.

[9] Solyaev Y (2022) Effective length scale parameters of the fiber-reinforced composites, Lobachevskii Journal of Mathematics **43**(7):1993-2002.

[10] La Valle G, Massoumi S (2022) A new deformation measure for micropolar plates subjected to in-plane loads, Continuum Mechanics and Thermodynamics **34**(1):243-257.

[11] Karathanasopoulos N, Reda H, Ganghoffer JF (2017) Designing two-dimensional metamaterials of controlled static and dynamic properties, Computational Materials Science **138**:323-332.

[12] De Cicco S, De Angelis F (2020) A plane strain problem in the theory of elastic materials with voids, Mathematics and Mechanics of Solids **25**(1):46-59.

[13] Michell AGM (1904) LVIII The limits of economy of material in frame-structures, The London, Edinburgh, and Dublin Philosophical Magazine and Journal of Science **8**(47):589-597.

[14] Abali BE, Barchiesi E (2021) Additive manufacturing introduced substructure and computational determination of metamaterials parameters by means of the asymptotic homogenization, Continuum Mechanics and Thermodynamics **33**(4):993-1009.

[15] Stilz M, Plappert D, Gutmann F, Hiermaier S (2022) A 3D extension of pantographic geometries to obtain metamaterial with semi-auxetic properties, Mathematics and Mechanics of Solids **27**(4):673-686.
[16] Yang H, Abali BE, Timofeev D, Müller WH (2020) Determination of metamaterial parameters by means of a homogenization approach based on asymptotic analysis, Continuum Mechanics and Thermodynamics **32**(5):1251-1270.
[17] Barchiesi E, dell'Isola F, Seppecher P, Turco E (2022) A beam model for duoskelion structures derived by asymptotic homogenization and its application to axial loading problems, European Journal of Mechanics-A/Solids **98**:104,848.
[18] Vangelatos Z, Gu GX, Grigoropoulos CP (2019) Architected metamaterials with tailored 3D buckling mechanisms at the microscale, Extreme Mechanics Letters **33**:100,580.
[19] Barchiesi E, Spagnuolo M, Placidi L (2019) Mechanical metamaterials: a state of the art, Mathematics and Mechanics of Solids **24**(1):212-234.
[20] dell'Isola F, Seppecher P, Alibert JJ, et al (2019) Pantographic metamaterials: an example of mathematically driven design and of its technological challenges, Continuum Mechanics and Thermodynamics **31**(4):851-884.
[21] Laudato M, Manzari L (2020) Linear dynamics of 2D pantographic metamaterials: numerical and experimental study, In: Developments and novel approaches in biomechanics and metamaterials, Springer, Cham, pp 353-375.
[22] Laudato M, Barchiesi E (2019) Non-linear dynamics of pantographic fabrics: modelling and numerical study, In: Wave dynamics, mechanics and physics of microstructured metamaterials, Springer, Cham, pp 241-254.
[23] Laudato M, Manzari L, Barchiesi E, Di Cosmo F, Göransson P (2018) First experimental observation of the dynamical behavior of a pantographic metamaterial, Mechanics Research Communications **94**:125-127.
[24] Engelbrecht J, Berezovski A, Pastrone F, Braun M (2005) Waves in microstructured materials and dispersion, Philosophical Magazine **85**(33-35):4127-4141.
[25] Eugster SR (2022) Numerical analysis of nonlinear wave propagation in a pantographic sheet, Mathematics & Mechanics of Complex Systems **9**:293-310.
[26] Turco E, Barchiesi E, dell'Isola F (2022) A numerical investigation on impulse-induced nonlinear longitudinal waves in pantographic beams, Mathematics and Mechanics of Solids **27**(1):22-48.
[27] Fedele R (2022) Piola's approach to the equilibrium problem for bodies with second gradient energies. Part I: First gradient theory and differential geometry, Continuum Mechanics and Thermodynamics **34**(2):445-474.
[28] Fedele R (2022) Third-gradient continua: nonstandard equilibrium equations and selection of work conjugate variables, Mathematics and Mechanics of Solids **27**(10):2046-2072.
[29] Rezaei N, Barchiesi E, Timofeev D, Tran CA, Misra A, Placidi L (2022) Solution of a paradox related to the rigid bar pull-out problem in standard elasticity, Mechanics Research Communications **126**:104,015
[30] Eremeyev VA, Lurie SA, Solyaev YO, dell'Isola F (2020) On the well posedness of static boundary value problem within the linear dilatational strain gradient elasticity, Zeitschrift für angewandte Mathematik und Physik **71**(6):1-16.

[31] Steigmann DJ, dell'Isola F (2015) Mechanical response of fabric sheets to three-dimensional bending, twisting, and stretching, Acta Mechanica Sinica **31**(3):373-382.
[32] Giorgio I, Rizzi NL, Turco E (2017) Continuum modelling of pantographic sheets for out-of-plane bifurcation and vibrational analysis, Proceedings of the Royal Society A: Mathematical, Physical and Engineering Sciences **473**(2207):20170,636.
[33] Shirani M, Luo C, Steigmann DJ (2019) Cosserat elasticity of lattice shells with kinematically independent flexure and twist, Continuum Mechanics and Thermodynamics **31**(4):1087-1097.
[34] Giorgio I, Ciallella A, Scerrato D (2020) A study about the impact of the topological arrangement of fibers on fiber-reinforced composites: some guidelines aiming at the development of new ultra-stiff and ultra-soft metamaterials, International Journal of Solids and Structures **203**:73-83.
[35] Giorgio I (2021) Lattice shells composed of two families of curved Kirchhoff rods: an archetypal example, topology optimization of a cycloidal metamaterial, Continuum Mechanics and Thermodynamics **33**(4):1063-1082.
[36] Spagnuolo M, Cazzani AM (2021) Contact interactions in complex fibrous metamaterials, Continuum Mechanics and Thermodynamics **33**(4):1873-1889.
[37] Spagnuolo M, Peyre P, Dupuy C (2019) Phenomenological aspects of quasi-perfect pivots in metallic pantographic structures, Mechanics Research Communications **101**:103,415.
[38] Ciallella A, Pasquali D, D'Annibale F, Giorgio I (2022) Shear rupture mechanism and dissipation phenomena in bias-extension test of pantographic sheets: Numerical modeling and experiments, Mathematics and Mechanics of Solids **27**(10):2170-2188.
[39] Ciallella A, D'Annibale F, Del Vescovo D, Giorgio I (2022) Deformation patterns in a second-gradient lattice annular plate composed of "spira mirabilis" fibers, Continuum Mechanics and Thermodynamics DOI 10.1007/s00161-022-01169-6.
[40] Jamun Kumar N, Dhas B, Srinivasa AR, Reddy JN, Roy D (2022) A novel four-field mixed FE approximation for Kirchhoff rods using Cartan's moving frames, Computer Methods in Applied Mechanics and Engineering **402**:115,094.
[41] Harsch J, Capobianco G, Eugster SR (2021) Finite element formulations for constrained spatial nonlinear beam theories, Mathematics and Mechanics of Solids **26(**12):1838-1863.
[42] Greco L (2020) An iso-parametric G^1-conforming finite element for the nonlinear analysis of Kirchhoff rod. Part I: the 2D case, Continuum Mechanics and Thermodynamics **32**:1473–1496.
[43] Schulte J, Dittmann M, Eugster SR, Hesch S, Reinicke T, dell'Isola F, Hesch C (2020) Isogeometric analysis of fiber reinforced composites using Kirchhoff-Love shell elements, Computer Methods in Applied Mechanics and Engineering **362**:112,845.
[44] Maurin F, Greco F, Desmet W (2019) Isogeometric analysis for nonlinear planar pantographic lattice: discrete and continuum models, Continuum Mechanics and Thermodynamics **31**(4):1051-1064.

[45] Greco L, Cuomo M, Contrafatto L (2018) A reconstructed local B formulation for isogeometric Kirchhoff-Love shells, Computer Methods in Applied Mechanics and Engineering **332**:462-487.

[46] Greco L, Cuomo M, Castello D, Scrofani A (2022) An updated lagrangian Bézier finite element formulation for the analysis of slender beams, Mathematics and Mechanics of Solids **27**(10):2110-2138.

[47] Greco L, Scrofani A, Cuomo M (2021) A non-linear symmetric G1-conforming Bézier finite element formulation for the analysis of Kirchhoff beam assemblies. Computer Methods in Applied Mechanics and Engineering **387**:114,176.

[48] Cazzani A, Malagù M, Turco E (2016) Isogeometric analysis of plane-curved beams, Mathematics and Mechanics of Solids **21**(5):562-577.

[49] Turco E, Barchiesi E, Ciallella A, dell'Isola F (2022) Nonlinear waves in pantographic beams induced by transverse impulses, Wave Motion **115**:103064.

[50] Turco E (2022) Modeling of three-dimensional beam nonlinear vibrations generalizing Hencky's ideas, Mathematics and Mechanics of Solids **27**(10):1950-1973.

[51] Turco E (2019) Numerically driven tuning of equilibrium paths for pantographic beams, Continuum Mechanics and Thermodynamics **31**(6):1941-1960.

[52] Barchiesi E, dell'Isola F, Bersani AM, Turco E (2021) Equilibria determination of elastic articulated duoskelion beams in 2D via a Riks-type algorithm., International Journal of Non-Linear Mechanics **128**:1-24.

[53] Eremeyev VA, Turco E (2020) Enriched buckling for beam-lattice metamaterials, Mechanics Research Communications **103**:103,458.

[54] Yildizdag ME, Placidi L, Turco E (2022) Modeling and numerical investigation of damage behavior in pantographic layers using a hemivariational formulation adapted for a Hencky-type discrete model, Continuum Mechanics and Thermodynamics DOI 10.1007/s00161-022-01154-z

[55] dell'Erba R (2019) Swarm robotics and complex behaviour of continuum material, Continuum Mechanics and Thermodynamics **31**(4):989-1014.

[56] dell'Erba R (2018) Position-based dynamic of a particle system: a configurable algorithm to describe complex behaviour of continuum material starting from swarm robotics, Continuum Mechanics and Thermodynamics **30**(5):1069-1090.

[57] Rosi G, Placidi L, Auffray N (2018) On the validity range of strain-gradient elasticity: a mixed static-dynamic identification procedure, European Journal of Mechanics-A/Solids **69**:179-191.

[58] Fantuzzi N, Tornabene F, Bacciocchi M, Dimitri R (2017) Free vibration analysis of arbitrarily shaped functionally graded carbon nanotube-reinforced plates, Composites Part B: Engineering **115**:384-408.

[59] Spagnuolo M, Yildizdag ME, Andreaus U, Cazzani AM (2020) Are higher-gradient models also capable of predicting mechanical behavior in the case of wide-knit pantographic structures? Mathematics and Mechanics of Solids DOI 10.1177/1081286520937339